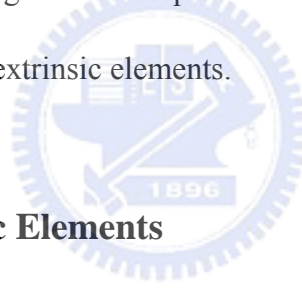


## Chapter 2

### Small-Signal Model Parameter Extraction Method

In this chapter, we introduce a new parameter extraction technique for small-signal HBT modeling. Figure 2-1 shows the small-signal equivalent circuit of a SiGe HBT under forward active mode operation. The model is based on the well-known hybrid- $\pi$  equivalent circuit with a three-element substrate network adding a parallel RC block connected in series with collector-substrate capacitance [12]. The equivalent circuit is divided into two parts, the inner part (in the dashed box) containing the bias-dependent intrinsic elements, and the outer part with the mostly bias-independent extrinsic elements.



#### 2.1 Extraction of Extrinsic Elements

To extract the equivalent circuit parameters, pad parasitics are carefully removed from measured S-parameters through a de-embedding procedure using an “open” test pattern. Some remaining parasitics not removed in the de-embedding procedure such as parasitic capacitances, pad inductances and series resistances are relatively small, but lead eventually to the errors in extracting intrinsic elements. Thus, their values should be determined carefully. After removing the residual parasitics, the extraction of substrate network parameters and subsequently the intrinsic parameters can then be performed.

##### 2.1.1 Extraction of pad inductances and series resistances

As reported in [13], the extraction of series resistances and pad inductances is made by

biasing the SiGe HBTs in “over-driven  $I_B$ ” bias condition where the base-collector and base-emitter junctions are in the forward bias condition. At high base current density, the base-emitter and base-collector dynamic resistances tend to be nearly zero and the junction capacitances become quite large. In such bias condition (collector voltage,  $V_{CE}=0$  and driving large forward base current,  $I_B$ ), the SiGe HBTs can be represented as a simple T-equivalent circuit consisting only of external base, emitter and collector series resistances and pad inductances as shown in Fig. 2-2. The Z-parameters of the equivalent circuit in Fig. 2-2 are defined by the following equation:

$$\begin{bmatrix} Z_{11} & Z_{12} \\ Z_{21} & Z_{22} \end{bmatrix} = \begin{bmatrix} R_{bx} + R_e + j\omega(L_b + L_e) & R_e + j\omega L_e \\ R_e + j\omega L_e & R_c + R_e + j\omega(L_c + L_e) \end{bmatrix} \quad (2-1)$$

The series resistances are determined at low frequency from the real parts of the Z-parameters and are show as

$$\begin{bmatrix} R_{bx} \\ R_c \\ R_e \end{bmatrix} = \begin{bmatrix} \text{Re}(Z_{11} - Z_{12}) \\ \text{Re}(Z_{22} - Z_{21}) \\ \text{Re}(Z_{12}) \end{bmatrix}. \quad (2-2)$$

At high base current densities, base-emitter and base-collector dynamic resistances became very small and  $\text{Re}(Z_{11}-Z_{12})$ ,  $\text{Re}(Z_{22}-Z_{21})$ , and  $\text{Re}(Z_{12})$  decrease linearly as a function of  $1/I_B$ , as shown in Fig. 2-3(a). The Y-axis interception for infinite large base currents yields the values of  $R_{bx}$ ,  $R_c$  and  $R_e$ .

The pad inductances can be described by the following equations:

$$\begin{bmatrix} \omega L_b \\ \omega L_c \\ \omega L_e \end{bmatrix} = \begin{bmatrix} \text{Im}(Z_{11} - Z_{12}) \\ \text{Im}(Z_{22} - Z_{21}) \\ \text{Im}(Z_{12}) \end{bmatrix}. \quad (2-3)$$

Using (2-3), one can easily get the values of  $L_b$ ,  $L_c$  and  $L_e$  from the slope when plotted  $\text{Im}(Z_{11}-Z_{12})$ ,  $\text{Im}(Z_{22}-Z_{21})$ , and  $\text{Im}(Z_{12})$  versus  $\omega$  at high base current density, as shown in Fig. 2-3(b).

### 2.1.2 Extraction of Parasitic Capacitances

The parasitic capacitances can be estimated from the SiGe HBTs under cutoff mode operation [14]. Under such bias conditions ( $V_{CE}=0$  and reverse and/or low forward base voltage,  $V_{BE}$ ), the effects of series resistances, dynamic resistance, and transconductance are negligible compared with those of the capacitance elements at low frequency range. The SiGe HBTs equivalent circuit of Fig. 2-1 is then reduced to capacitance elements only, and can be represented by the equivalent circuit shown in Fig. 2-4.

From the Y-parameters analysis of this circuit, we get

$$\text{Im}(Y_{11} + Y_{12}) = \omega(C_{bep} + C_{\pi}) \quad (2-4)$$

$$\text{Im}(-Y_{12}) = \omega(C_{bcp} + C_{bcx} + C_{bci}). \quad (2-5)$$

In (2-4) and (2-5), the base-emitter junction capacitance  $C_{\pi}$ , and the total base-collector junction capacitance,  $C_{bcx}+C_{bci}$ , are considered to be bias dependent, while the parasitic capacitances  $C_{bep}$  and  $C_{bcp}$  are bias independent elements. Both the base-emitter and total base-collector junction capacitances can be described by the well-known expression  $C_j = C_{j0}(1 - V_j/V_{pj})^{-m_j}$  where  $C_j$  is the junction capacitance,  $C_{j0}$  is the junction capacitance at zero bias,  $V_j$  is the applied reverse voltage,  $V_{pj}$  is built-in voltage of the junction, and  $m_j$  is the exponent.

Fig. 2-5 shows the extraction of the parasitic capacitances,  $C_{bep}$  and  $C_{bcp}$ , are carried out

by fitting  $\text{Im}(Y_{11}+Y_{12})/\omega$  and  $\text{Im}(-Y_{12})/\omega$  to the expression  $(1-V_{be}/V_{bi})^{-m_{be}}$  and  $(1-V_{bc}/V_{ci})^{-m_{bc}}$ , respectively. By varying the parameters  $V_{bi}$  and  $m_{be}$  until  $\text{Im}(Y_{11}+Y_{12})/\omega$  shows a linear behavior as a function of  $(1-V_{be}/V_{bi})^{-m_{be}}$ , the extrapolated Y-axis interception yields the value of parasitic capacitance  $C_{bep}$ . The obtained value of  $C_{bep}$  is about 23.00 fF. In a similar way, the extracted  $C_{bcp}$  is about 0 fF.

## 2.2 Extraction of Substrate Network Parameters

Under the bias conditions ( $V_{BE}=0$  and forward and/or low reverse collector voltage), the substrate network parameters can be estimated from the Y-parameters analysis of the equivalent circuit shown in Fig. 2-1. After removing the extrinsic inductances, parasitic capacitances, extrinsic base resistance and collector resistance, the equivalent circuit of Fig. 2-1 is reduced to that of Fig. 2-6(a). The extrinsic inductances,  $L_b$ ,  $L_c$  and  $L_e$  are de-embedded firstly by

$$[Z_i] = [Z] - \begin{bmatrix} j\omega(L_b + L_e) & j\omega L_e \\ j\omega L_e & j\omega(L_c + L_e) \end{bmatrix}. \quad (2-6)$$

where  $[Z]$  denotes impedance parameters of the device under test (DUT) after de-embedding the “open” test pattern. After transforming  $[Z_i]$  into its admittance matrix  $[Y_i]$ , the parasitic capacitances,  $C_{bep}$  and  $C_{bcp}$  are removed by

$$[Y_j] = [Y_i] - \begin{bmatrix} j\omega(C_{bep} + C_{bcp}) & -j\omega C_{bcp} \\ -j\omega C_{bcp} & j\omega C_{bcp} \end{bmatrix}. \quad (2-7)$$

Converting  $[Y_j]$  to its impedance matrix  $[Z_j]$ , then  $R_{bx}$  and  $R_C$  can be subtracted by

$$[Z_k] = [Z_j] - \begin{bmatrix} R_{bx} & 0 \\ 0 & R_c \end{bmatrix}. \quad (2-8)$$

Finally, convert  $[Z_k]$  to  $[Y_k]$  to obtain the information containing the frequency response of intrinsic HBT and substrate network.

In this study, the substrate network  $Y_{sub}$ , is constituted of substrate-collector depletion capacitance  $C_{sub}$ , substrate resistance  $R_{bk}$  and bulk capacitance  $C_{bk}$  accounting for Si dielectric behavior. For simplicity, the influence of emitter resistance  $R_e$  has been neglected where the approximation is valid for  $(\omega R_e C_\pi)^2 = 1$ . We transform the intrinsic part of the device equivalent circuit ( $R_{bi}$ ,  $C_\pi$ ,  $C_{bci}$ ) using the well-known  $T \leftrightarrow \Pi$  transformations shown in detail in the right side of Fig. 2-6(b). Observing  $[Y_k]$  shown in Fig. 2-6(b), we can derive

$$Y_{22,k} + Y_{21,k} = Y_{sub} + Y_3 \quad (2-9)$$

where

$$Y_{sub} = \frac{\omega^2 R_{bk} C_{sub}^2}{1 + \omega^2 R_{bk}^2 (C_{bk} + C_{sub})^2} + j\omega C_{sub} \left( \frac{1 + \omega^2 R_{bk}^2 C_{bk} (C_{bk} + C_{sub})}{1 + \omega^2 R_{bk}^2 (C_{bk} + C_{sub})^2} \right) \quad (2-10)$$

$$Y_3 = \frac{-\omega^2 C_{bci} C_\pi R_{bi}}{1 + \omega^2 R_{bi}^2 (C_{bci} + C_\pi)^2} + j \frac{\omega^3 C_{bci} C_\pi (C_{bci} + C_\pi) R_{bi}^2}{1 + \omega^2 R_{bi}^2 (C_{bci} + C_\pi)^2}. \quad (2-11)$$

From (2-9), it is clear that  $(Y_{22,k} + Y_{21,k})$  deviates from  $Y_{sub}$  by an additional term,  $Y_3$ , which is constituted of the intrinsic circuit elements. If the extraction of substrate network parameters is performed on  $Y_{22,k} + Y_{21,k}$ , the conductance of substrate network will be underestimated and the susceptance of substrate network will be overestimated.

To extract substrate network parameters,  $Y_3$  should be determined first. Observing  $Y_k$  shown in Fig. 2-6(a),  $R_{bi}$  and  $C_\pi$  can be obtained as

$$R_{bi} = \operatorname{Re} \left[ \frac{1}{Y_{11,k} + Y_{12,k}} \right] \frac{\operatorname{Re}(Y_{11,k} + Y_{12,k})}{\operatorname{Re}(Y_{11,k})} \quad (2-12)$$

$$\omega C_{\pi} = -\operatorname{Im} \left( \frac{1}{Y_{11,k} + Y_{12,k}} \right)^{-1}. \quad (2-13)$$

Fig. 2-7 and 2-8 show the  $R_{bi}$  extracted from (2-12) is nearly constant and the  $\omega C_{\pi}$  extracted from (2-13) is linear. We find  $R_{bi}=21.37 \Omega$  and  $C_{\pi}=75.69 \text{ fF}$  at  $V_{CE}=3.0 \text{ V}$ , and  $V_{BE}=0 \text{ V}$  for the  $4 \times 0.24 \times 32 \mu\text{m}^2$  SiGe HBT. In the low frequency range,  $\operatorname{Re}(Y_{11,k})$  can be approximately rewritten as (2-14)

$$\operatorname{Re}(Y_{11,k}) = \frac{\omega^2 R_{bi} (C_{\pi} + C_{bci})^2}{1 + \omega^2 R_{bi}^2 (C_{\pi} + C_{bci})^2} : \omega^2 R_{bi} (C_{\pi} + C_{bci})^2 \Big|_{\text{at low frequency}} \quad (2-14)$$

under the assumption,  $\omega^2 R_{bi}^2 (C_{\pi} + C_{bci})^2 = 1$ , it can be expressed a typical result of (2-14) at  $V_{CE}=3.0\text{V}$ , and  $V_{BE}=0\text{V}$  for a  $4 \times 0.24 \times 32 \mu\text{m}^2$  SiGe HBT .The intrinsic base-collector capacitance  $C_{bci}$  can be extracted as  $6.293 \text{ fF}$  from  $C_{bci} = \beta^{0.5} R_{bi}^{-0.5} - C_{\pi}$  where  $\beta$  is the slope of  $\operatorname{Re}(Y_{11,k})$  versus  $\omega^2$  plot which shows at Fig. 2-9. Once  $R_{bi}$ ,  $C_{\pi}$  and  $C_{bci}$  are obtained,  $Y_3$  and  $Y_{\text{sub}}$  can be derived from (2-11) and (2-10), respectively.

From (2-9), it indicates that  $Y_3$  (or intrinsic circuit elements) indeed affects the measured  $(Y_{22,k}+Y_{21,k})$ . Figs. 10 and 11 show the comparison between measured  $(Y_{22,k}+Y_{21,k})$  and  $Y_{\text{sub}}$  for a SiGe HBT. Due to the internal feedback signal through  $Y_3$ ,  $\operatorname{Re}(Y_{22,k}+Y_{21,k})$  and  $\operatorname{Im}(Y_{22,k}+Y_{21,k})/\omega$  show a deviation from  $\operatorname{Re}(Y_{\text{sub}})$  and  $\operatorname{Im}(Y_{\text{sub}})/\omega$  as operation frequency beyond 5 GHz and 10 GHz, respectively.

To extract the substrate network parameters, two linear equations are derived from  $Y_{\text{sub}}$  and are shown as

$$\frac{\text{Im}(Y_{sub})}{\omega \text{Re}(Y_{sub})} = \frac{1}{\omega^2 R_{bk} C_{sub}} + R_{bk} \frac{C_{bk} (C_{bk} + C_{sub})}{C_{sub}} = \frac{1}{\omega^2} k_1 + k_2 \quad (2-15)$$

$$\frac{1}{\text{Re}(Y_{sub})} = \frac{1}{\omega^2 R_{bk} C_{sub}^2} + R_{bk} \left( \frac{C_{bk} + C_{sub}}{C_{sub}} \right)^2 = \frac{1}{\omega^2} m_1 + m_2. \quad (2-16)$$

As indicated in Fig. 2-12,  $k_1$  and  $m_1$  can be obtained from the linear regression of (2-15) and (2-16). In Fig. 2-12,  $C_{sub}$  and  $R_{bk}$  are calculated as 15.65 fF and 164.61  $\Omega$  from  $k_1/m_1$  and  $m_1/(k_1)^2$ , respectively. Having determined  $C_{sub}$  and  $R_{bk}$ ,  $C_{bk}$  is calculated as 25.22fF from  $C_{bk} = (C_{sub}^2 / (R_{bk} \text{Re}(Y_{sub})) - (\omega R_{bk})^{-2})^{0.5} - C_{sub}$  [15]. Fig. 2-13 shows the collector-voltage dependence of the extracted substrate network parameters. The slightly increased  $C_{bk}$  and slightly decreased  $R_{bk}$  probably indicate the reduction of Si bulk region due to the increase of the collector-substrate depletion width [12].

After extraction of substrate network parameters,  $Y_{sub}$  is de-embedded through the following equation:

$$[Y_m] = [Y_k] - \begin{bmatrix} 0 & 0 \\ 0 & Y_{sub} \end{bmatrix}. \quad (2-17)$$

Finally, convert  $[Y_m]$  to  $[Z_m]$ , de-embed  $R_e$  through the following equation, and re-convert  $[Z_n]$  to  $[Y_n]$  to obtain the admittance parameters of intrinsic HBT

$$[Z_n] = [Z_m] - \begin{bmatrix} R_e & R_e \\ R_e & R_e \end{bmatrix} \quad (2-18).$$

### 2.3 Extraction of Intrinsic Circuit Elements

Usually, the admittance parameters of the intrinsic HBT in common-emitter configuration,  $[Y_n]$  are used to extract intrinsic circuit elements [16][17]. A much simpler set of equations is

obtained, if the equivalent circuit of the intrinsic HBT is transformed to its common-collector configuration as shown in Fig. 2-14 [18][19]. After two-port matrix operations, we arrive at the following ABCD-parameters  $[A_c]$  of the intrinsic HBT

$$A_{c,11} = 1 + R_{bi}Y_{bc} \quad (2-19)$$

$$A_{c,12} = \frac{1}{g_m + Y_\pi} (1 + R_{bi}Y_{bc} + R_{bi}Y_\pi) \quad (2-20)$$

$$A_{c,21} = Y_{bc} + Y_{ex} + R_{bi}Y_{ex}Y_{bc} \quad (2-21)$$

$$A_{c,22} = \frac{1}{g_m + Y_\pi} [Y_{ex} (1 + R_{bi}Y_{bc} + R_{bi}Y_\pi) + Y_{bc} + Y_\pi] \quad (2-22)$$

where  $g_m = g_{m0} \exp(-j\omega\tau)$ ,  $Y_\pi = 1/R_\pi + j\omega C_\pi$ ,  $Y_{bc} = j\omega C_{bci}$ , and  $Y_{ex} = j\omega C_{bcx}$ . The advantage of transforming the intrinsic circuit into its common-collector configuration is that some circuit parameters such as  $g_m$  and  $Y_\pi$  only appear in  $A_{c,12}$  and  $A_{c,22}$  and this facilitates the extraction of some intrinsic circuit parameters.

### 2.3.1 Extraction of $R_{bi}$ , $C_{bci}$ , $C_\pi$ , and $C_{bcx}$

From (2-20) and (2-22), the well-known ABCD-parameter formulation for extraction of intrinsic base resistance,  $R_{bi}$ , given in [18] is shown as

$$\operatorname{Re} \left( \frac{A_{c,12}}{A_{c,22}} \right) = \frac{\omega^2 R_{bi} (C_{bci} + C_\pi)^2}{\omega^4 R_{bi}^2 C_{ex}^2 (C_{bci} + C_\pi)^2 + \omega^2 (C_{bci} + C_\pi + C_{ex})^2}. \quad (2-23)$$

Since the  $\omega^4$  term in denominator is much small than the  $\omega^2$  term at middle to high frequency range, (2-23) is simplified to

$$\operatorname{Re} \left( \frac{A_{c,12}}{A_{c,22}} \right) : R_{bi} \frac{(C_{bci} + C_\pi)^2}{(C_{bci} + C_\pi + C_{ex})^2} \Big|_{\text{at middle to high frequency}} \quad (2-24)$$



which set up the lower limit of  $R_{bi}$ . Another equation for extraction of  $R_{bi}$  can be obtained from (2-19) to (2-22)

$$\begin{aligned} \operatorname{Re}\left(\frac{A_{c,12}}{|A_c|}\right) &= R_{bi} \left(1 + \frac{C_{bci}}{C_\pi}\right) + \frac{1}{\omega^2 R_{be} C_\pi^2} \\ &: R_{bi} \left(1 + \frac{C_{bci}}{C_\pi}\right) \Big|_{\text{at middle to high frequency}} \end{aligned} \quad (2-25)$$

where  $|A_c|$  denotes  $(A_{c,11}A_{c,22} - A_{c,12}A_{c,21})$ . It is clear that (2-25) set up the upper limit of  $R_{bi}$ . Typical results of (2-24) and (2-25) are shown in Fig. 2-15. We find the lower limit and upper limit of  $R_{bi}$  are 17.31  $\Omega$  and 14.85  $\Omega$ , respectively, at  $I_B=9.136 \mu\text{A}$ , and  $I_C=1.516 \text{ mA}$  and  $V_{CE}=3.0 \text{ V}$  for the  $4 \times 0.24 \times 32 \mu\text{m}^2$  SiGe HBT. The  $R_{bi}$  estimated from (2-24) is then applied to obtain intrinsic base-collector capacitance,  $C_{bci}$ , through following equation

$$\operatorname{Im}(A_{c,11}) = \omega R_{bi} C_{bci}. \quad (2-26)$$

Fig. 2-16 shows the value of  $R_{bi} C_{bci}$  is calculated from the slope of (2-26) when plotted versus the angular frequency  $\omega$ . It should be noted that the adopted  $R_{bi}$  from (2-24) only serve as an initial value and it will be corrected in the accuracy improvement procedure.

By examing (2-19) to (2-22), we can extract intrinsic base-emitter capacitance,  $C_\pi$ , through following equation

$$\begin{aligned} \operatorname{Im}\left(\frac{A_{c,12}}{|A_c|}\right) &= \frac{\omega R_{be} C_{bci} R_{bi} - \omega R_{be}^2 C_\pi}{1 + (\omega R_{be} C_\pi)^2} \\ &: \frac{-1}{\omega C_\pi} \left(1 - \frac{R_{bi} C_{bci}}{R_{be} C_\pi}\right) \Big|_{\text{at middle to high frequency}} \cdot \\ &: \frac{-1}{\omega C_\pi} \Big|_{\text{at middle to high frequency}} \end{aligned} \quad (2-27)$$

The value of  $C_\pi$  is calculated as 410.31fF from the slope of (2-27) when plotted versus  $1/\omega$ , as

shown in Fig. 2-17.

To extract the extrinsic base-collector capacitance,  $C_{bcx}$ , we obtain following equation by inspecting (2-19) and (2-21)

$$\text{Im}\left(\frac{A_{c,11}}{A_{c,21}}\right) = \frac{\omega^3 R_{bi}^3 C_{bci}^2 C_{bcx} - \omega(C_{bci} + C_{bcx})}{\omega^4 (R_{bi} C_{bci} C_{bcx})^2 + \omega^2 (C_{bci} + C_{bcx})^2}. \quad (2-28)$$

In the low to middle frequency range, the  $\omega^4$  term in denominator is much smaller than the  $\omega^2$  term. Also, the  $\omega^3$  term in numerator is much smaller than the  $\omega$  term. Thus, (2-28) is simplified to

$$\text{Im}\left(\frac{A_{c,11}}{A_{c,21}}\right) : \frac{-1}{\omega(C_{bci} + C_{bcx})} \Big|_{\text{at low to middle frequency}}. \quad (2-29)$$

The value of  $C_{bci}+C_{bcx}$  is calculated from the slope of (2-29) when plotted versus  $1/\omega$ , as shown in Fig. 2-18. Since the value of  $C_{bci}$  has been previously determined,  $C_{bcx}$  is obtained by subtracting  $C_{bci}+C_{bcx}$  from  $C_{bci}$ .

### 2.3.2 Accuracy Improvement of $R_{bi}$ , $C_{bci}$ and $C_{bcx}$

In (2-26) and (2-29), we found that  $R_{bi}$  plays a significant role on the accuracy of extracted  $C_{bci}$  and subsequently the accuracy of extracted  $C_{bcx}$ . However, the estimated value of  $R_{bi}$  from (2-24) is lower than the real one. Thus, an accuracy improvement procedure is necessary and listed as follows:

- 1) The value of  $R_{bi}$  estimated from (2-24) is applied in the extraction of  $C_{bci}$  through (2-26).

The extraction results of  $C_{bci}$  is used in the extraction of  $C_{bcx}$  through (2-29).

2) The new lower limit and new upper limit of  $R_{bi}$  is obtained by taking extracted  $C_{bci}$  and  $C_{bcx}$  in the calculation of (2-30) and (2-31), respectively.

$$R_{bi}|_L = \frac{(C_{bci} + C_{\pi} + C_{bcx})^2}{(C_{bci} + C_{\pi})^2} \times \text{Re} \left( \frac{A_{c,12}}{A_{c,22}} \right) \Big|_{\text{at middle to high frequency}} \quad (2-30)$$

$$R_{bi}|_U = \left( 1 + \frac{C_{bci}}{C_{\pi}} \right)^{-1} \times \text{Re} \left( \frac{A_{c,12}}{|A_c|} \right) \Big|_{\text{at middle to high frequency}} \quad (2-31)$$

The calculated  $R_{bi}|_L$  is sent back to step 1) to repeat the calculation to step 2). Once the the difference between  $R_{bi}|_L$  and  $R_{bi}|_U$  is minimum,  $R_{bi}|_L$  is treated as the final  $R_{bi}$ . A typical results of proposed accuracy improvement procedure for the  $4 \times 0.24 \times 32 \mu\text{m}^2$  SiGe at  $I_B=9.136 \mu\text{A}$ , and  $I_C=1.516 \text{ mA}$  and  $V_{CE}=3.0 \text{ V}$ , is shown in Table I. The difference between  $R_{bi}|_L$  and  $R_{bi}|_U$  decreases very quickly in the first four iterations. The extracted  $R_{bi}$ ,  $C_{bci}$ , and  $C_{bcx}$  are found to be  $16.510 \Omega$ ,  $5.864 \text{ fF}$ , and  $14.66 \text{ fF}$ , respectively.

### 2.3.3 Extraction of $R_{\pi}$ , $g_{m0}$ and $\tau$

The remaining unknowns are intrinsic transconductance,  $g_{m0}$ , excess phase delay,  $\tau$ , and base-emitter resistance,  $R_{\pi}$  which can be calculated as follows.

$$\frac{1}{R_{\pi}} = \text{Re} \left( \frac{A_{c,11}|A_c|}{A_{c,12} - |A_c|R_{bi}} \right) \quad (2-32)$$

The value of  $R_{\pi}$  is estimated as  $1.349 \text{ k}\Omega$  at  $I_B=9.136 \mu\text{A}$ , and  $I_C=1.516 \text{ mA}$  and  $V_{CE}=3.0\text{V}$  for the  $4 \times 0.24 \times 32 \mu\text{m}^2$  SiGe HBT, as shown in Fig. 2-19.

The transconductance,  $g_{m0}$ , and the excess phase delay,  $\tau$ , is calculated as follows.

$$g_m = \frac{1 - |A_c|}{|A_c|} Y_\pi \quad (2-33)$$

$$g_{m0} = \sqrt{\text{Re}(g_m)^2 + \text{Im}(g_m)^2} \quad (2-34)$$

$$\tau = -\tan^{-1}\left(\frac{\text{Im}(g_m)}{\text{Re}(g_m)}\right) \times \frac{1}{\omega}. \quad (2-35)$$

Figures 2-20 show the extracted results for the  $4 \times 0.24 \times 32 \mu\text{m}^2$  SiGe HBT biased at  $I_B = 9.136 \mu\text{A}$ , and  $I_C = 1.516 \text{ mA}$  and  $V_{CE} = 3.0 \text{ V}$ . The value of  $R_\pi$  is estimated as  $1.349 \text{ k}\Omega$ . The extracted  $g_{m0}$ , and  $\tau$  are  $53.58 \text{ mS}$  and  $2.103 \text{ psec}$ , respectively. Both of  $g_{m0}$ , and  $\tau$  are found to be nearly constant in the interested frequency range.



### 2.3.4 Discrepancy between measurement and simulation

Figure 2-21 and 2-22 show the comparisons between the measured and calculated S-parameters for  $V_{CE} = 3\text{V}$ ,  $V_{BE} = 0.83\text{V}$ ,  $I_C = 1.516\text{mA}$ , and  $I_B = 9.316\mu\text{A}$ . Excellent agreements over the whole frequency range were obtained. The total error in the S-parameter calculated by following function [10][20].

$$E_{\text{tot}} = 100 \times \frac{1}{4N_{\text{freq}}} \sum_{i,j} \sum_{\text{freq}} \frac{|S_{ij}^{\text{meas}} - S_{ij}^{\text{sim}}|^2}{|S_{ij}^{\text{meas}}|^2} \quad (2-36)$$

The residual discrepancies are about  $0.50766\%$  for the whole bias points. Therefore, we believe that the proposed method is an accurate extraction technique applicable to evaluate the process technology and optimize the transistor design.

# of iteration	$R_{bi L}(\Omega)$	$R_{bi H}(\Omega)$	$C_{bci}(fF)$	$C_{bcx}(fF)$	$\Delta R_{bi}(\Omega)$
1	14.85	17.31	4.7897	15.7303	2.46
2	15.936	17.110	4.8456	15.6744	1.174
3	15.967	17.108	4.8463	15.6737	1.141
4	15.966	17.108	4.8463	15.6737	1.142
5	15.966	17.108	4.8463	15.6737	1.142

**Table 2-1 Typical results of proposed accuracy improvement procedure for  $4 \times 0.24 \times 32 \mu m^2$  SiGe at  $V_{BE}=0.82$  V,  $V_{CE}=3$  V,  $I_B=9.136$   $\mu A$ , and  $I_C=1.516$  mA. The initial value of  $R_{bi|L}$ ,  $R_{bi|H}$ ,  $C_{bci}$ , and  $C_{bcx}$  are 14.85  $\Omega$ , 17.31  $\Omega$ , 4.7897 fF, and 15.7303 fF, respectively. The extracted value of  $R_{bi}C_{bci}$ ,  $C_\pi$  and  $C_{bci}+C_{bcx}$  are 82.91fsec, 410.31fF and 20.52fF, respectively.**

